Report on Pedestal Stability, Transport and ELM Issues for Snowmass Burning Plasma Candidates

Philip B. Snyder, General Atomics, 19 July 2002
Acknowledgments: H.R. Wilson, J. Drake, B. Rogers, A. Hubbard, J.D. Callen, R. Waltz, J. Kinsey, R. Groebner, A. Leonard

This report is prepared as a contribution to the uniform technical assessment of pedestal physics issues for the burning plasma candidates, ITER, FIRE, and Ignitor. Issues falling under both the MHD (P3) and transport (P4) topical groups are considered.

I. Introduction & Motivation

The term "pedestal" is used here to describe the sharp pressure gradient region just inside the magnetic separatrix (or limiter, if one is present) in H-mode operation. This region generally occupies approximately the outer 1-5% in normalized radius of the closed flux surface region, but is observed to have a disproportionately large impact on overall plasma performance [see e.g., Refs. 1-3].

The physics of the pedestal is expected to be critically important to the performance of burning plasma devices for two primary reasons. The first is the strong dependence, both observed and predicted by transport models, of core confinement on the pressure at the top of the pedestal (or "pedestal height"). Core transport models (e.g., GLF23, Multi-Mode, IFS-PPPL) take the pedestal height as an input parameter, and predict the resulting transport in the core. Because these models are "stiff" (transport increases rapidly above a critical gradient), the predicted core temperature, and hence fusion power or $Q=P_{fus}/P_{in}$, increases strongly with increasing pedestal height. For GLF23, the dependence is roughly $P_{fus}\sim\beta^2_{ped}$, where β_{ped} is the ratio of plasma to magnetic pressure at the top of the pedestal (see the transport section of this report for further details). Hence, transport code predictions for the burning plasma candidates can be restated in terms of the pedestal height (or at a given density, the pedestal temperature) requirements for a given level of fusion performance.

The second important pedestal physics issue is the presence of edge localized modes (ELMs). ELMs are repetitive magnetic perturbations in the pedestal vicinity, which transport bursts of particles, and usually also heat, across the separatrix and to the divertor plates [see e.g., Refs. 4-7]. While the ELMs themselves are generally benign in present experiments, large ELMs potentially pose a significant divertor erosion risk in burning plasma scale devices. Furthermore, ELMs appear to be a manifestation of magnetohydrodynamic instabilities driven by some combination of the strong pressure gradient and resulting bootstrap current in the pedestal region. These instabilities place constraints on the achievable pedestal height at a given transport barrier width, and thus constrain overall performance as discussed above. Developing a predictive understanding of the physics controlling ELMs and the pedestal height is an important goal for pedestal theory, and also a key motivation for building a burning plasma scale device to explore pedestal physics and establish a high pedestal, small ELM regime at relevant fusion reactor parameters.

While there has been significant recent progress in understanding certain aspects of pedestal physics, great uncertainty remains in many areas. In particular, the physics governing the L-H transition, and limiting the width of the resulting transport barrier is not well understood. As a result, a complete assessment of pedestal issues in the burning plasma candidates is challenging.

One area of recent progress has been in the tentative identification of ELMs with intermediate wavelength MHD instabilities. Theory/experiment comparisons on a number of experiments (DIII-D, Alcator C-Mod, Asdex-U, JET, JT-60U) have found that the onset of ELMs, and when measurable the wavelength and penetration depth of ELMs, are generally consistent, within experimental uncertainty, with the predicted onset and characteristics of MHD peeling-ballooning instabilities [see e.g., Refs. 8-13].

These peeling-ballooning instabilities are driven by the sharp pressure gradients, and resulting large bootstrap current in the pedestal region [see e.g., Refs. 13-14]. Field line bending stabilizes long wavelength modes, while short wavelengths are stabilized by a combination of second stability and FLR/diamagnetic effects, shifting the limiting modes to intermediate wavelengths (n~4-30). These intermediate-n modes impose constraints on the pedestal height, which are functions of the pedestal width, plasma shape, and plasma density. Within the ideal MHD framework, and the uncertainties in reconstructed or model equilibria, it is possible to quantitatively characterize these constraints using existing codes. Such characterizations have been useful in predicting observed trends in pedestal height, for example with plasma triangularity, squareness, and collisionality [e.g., Refs. 3,7,11-13] . While this is an active area of research, and a number of aspects, particularly the impact of sheared flow and non-ideal effects, remain to be fully investigated, it is nonetheless deemed useful to conduct an investigation of the MHD pedestal stability constraints in ITER, FIRE and Ignitor model equilibria. These calculations should provide an approximate feasibility check on the required pedestal heights predicted by the core transport modeling. They also provide a starting point for the modeling of non-ideal effects, and they can be combined with empirical or semi-empirical models of the pedestal width to yield very approximate predictions of achievable pedestal height in the candidate machines. Analysis of the most unstable wavelengths and mode penetration also provides input to models projecting ELM size.

Details of the construction of model equilibria with varying pedestal characteristics, and the characterization of ideal intermediate mode number (n) MHD pedestal stability limits are given in Section II. Non-ideal effects, including an assessment of diamagnetic stabilization using simple models, are considered in Section III. A summary of the pedestal stability study is given in Section IV, and implications, including brief discussion of empirical pedestal models, are discussed in Section V.

II. Assessment of Ideal MHD Pedestal Stability Constraints

II.a. Model Equilibria

In order to characterize pedestal MHD stability limits, a large number of equilibria must be constructed which incrementally vary the pedestal width and height. For these purposes the

details of the equilibrium deep in the core are relatively unimportant, but should be broadly consistent with expected profiles for each device.

Ignitor requires some special consideration, since its reference operation point is in L-mode. However, L-mode operation does not impact the performance predictions from core transport codes, which predict the required pressure values in the outer region, e.g., at the 95% flux surface (that is, the L-mode equivalent of the pedestal height), needed for good performance. Thus if one accepts the core transport predictions, one must either argue that these large outer region pressures are achievable in L-mode, or propose H-mode operation. In either case, the pedestal stability limits should provide a useful figure of merit. Furthermore, the Ignitor team has recently proposed possible H-mode scenarios. So, in the spirit of a uniform assessment, the stability constraints on H-mode pedestals will be studied in Ignitor just as in the other proposed devices. [It has been suggested that it would be useful to explore Ignitor operation at lower current (I_p~9MA), where H-mode operation is expected to be more easily achieved. Reduced current lowers I/aB and thus may lower the pedestal beta limit (Fig. 3b) somewhat, but a detailed pedestal stability investigation of a 9MA scenario awaits further work.]

Model equilibria have been constructed to match the global parameters for each machine given in Table 1. These should be consistent with the design parameters for the reference cases, except for small modifications to the density of FIRE.

	ITER	FIRE	Ignitor
B_t (T)	5.3	10	13
I_p (MA)	15	7.7	11
R (m)	6.2	2.14	1.33
a (m)	2.0	0.595	0.455
κ_a	1.85	2.0	1.8
δ_a	0.49	0.7	0.4
$\langle n_e \rangle (10^{20} m^{-3})$	1.0	3.6	9.5

Table 1: Reference parameters for the model equilibria

Density and temperature profiles are given a hyperbolic tangent shape in the pedestal [resembling measured profiles, see e.g. Refs. 3,1], and a simple polynomial dependence in the core:

$$n_e(\psi) = n_{sep} + a_{n0}\{\tanh[2(1-\psi_{mid})/\Delta] - \tanh[2(\psi-\psi_{mid})/\Delta]\} + a_{n1}[1-(\psi/\psi_{ped})^{\alpha_{n1}}]^{\alpha_{n2}}$$

$$T(\psi) = T_{sep} + a_{T0}\{\tanh[2(1-\psi_{mid})/\Delta] - \tanh[2(\psi-\psi_{mid})/\Delta]\} + a_{T1}[1-(\psi/\psi_{ped})^{\alpha_{T1}}]^{\alpha_{T2}}$$

where ψ is the normalized poloidal flux, and Δ is the pedestal width in ψ space. The constants a_0 and a_1 are chosen to give the desired pedestal and axis values, and α_0 and α_1 are chosen to approximately match expected core profiles from transport codes. For the baseline cases, $n_{ped}=0.71\langle n_e\rangle$, $n_0=1.1\langle n_e\rangle$, $n_{sep}=0.3\langle n_e\rangle$, $\alpha_{n0}=1$, $\alpha_{n1}=0.5$, $\alpha_{T0}=1$, $\alpha_{T1}=2$.

In the pedestal region, the parallel current is taken to be equal to the bootstrap current, as calculated using the Sauter collisional model [15]. In the core, where details of the current are

relatively unimportant, the profile is taken to have a simple polynomial form, with coefficients chosen to give a central q_0=1.05, and a total I_p as in Table 1.

A number of simplifications are made to simplify the equilibrium construction process, including up-down symmetry (while matching the given separatrix elongation and triangularity), and lack of true X-points.

II.b. Ideal MHD Pedestal Stability

To characterize the pedestal stability constraints, the pedestal width ( ) is varied, and at each value of , the pedestal temperature is increased incrementally (with the bootstrap current calculated self-consistently) until stability boundaries are crossed. Sample model ITER equilibrium profiles near the stability boundary at a pedestal width /a~0.03 are shown in Fig. 1.

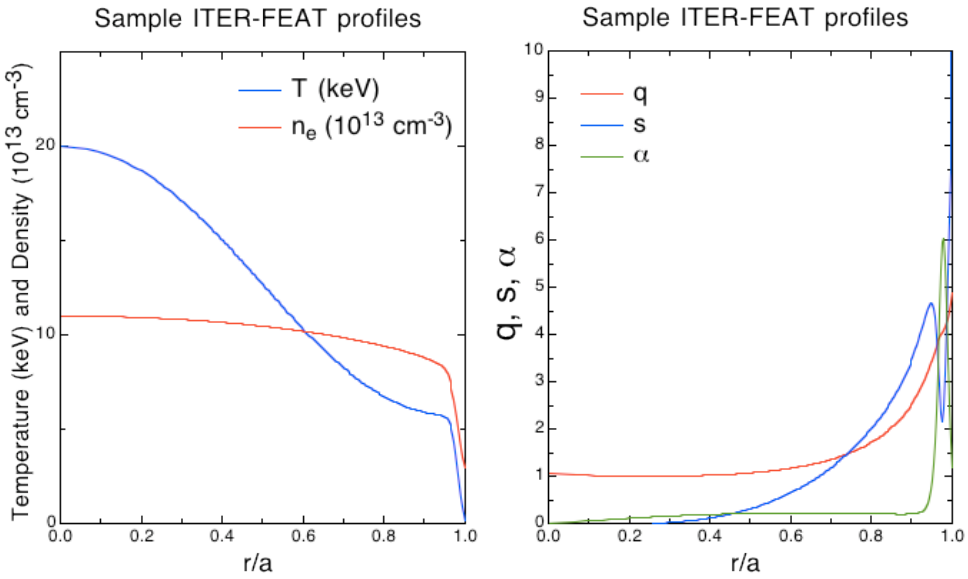

Figure 1: Equilibrium profiles for a sample ITER case with pedestal width of /a~0.03, and pedestal temperature T_{ped}~5keV.

The intermediate n (n>~5) MHD code ELITE [16,13] is used in the pedestal stability calculations. ELITE has been successfully benchmarked against the GATO [17] and MISHKA [18] codes, and allows efficient calculation of the pedestal stability bounds, and the growth rates and mode structures of the limiting instabilities [16,13]. A sampling of wavelengths, n=8,10,15,20,30, are studied, over the range expected to be most unstable. A finite growth rate threshold (/ $_A$>0.01) is used as a threshold for "instability," eliminating slow growing modes unlikely to trigger ELMs. The results presented in this report required the production of more than 1000 high resolution 2D equilibria, and more than 5000 intermediate-n MHD stability calculations.

The results of these calculations of intermediate-n ideal stability bounds on T_{ped} (at fixed n_{ped}) as a function of the pedestal width are given for each machine in Fig. 2. Note that at narrow pedestal widths, relatively high n modes are the most unstable for all 3 cases, while at wider

pedestal widths, high n modes become second stable in ITER and FIRE, and modes in the range n~10-20 are most unstable. The maximum stable pedestal temperature is found to be a monotonically increasing function of pedestal width, but the dependence is sub-linear, particularly at small widths, as can be seen most clearly in Fig. 2c.

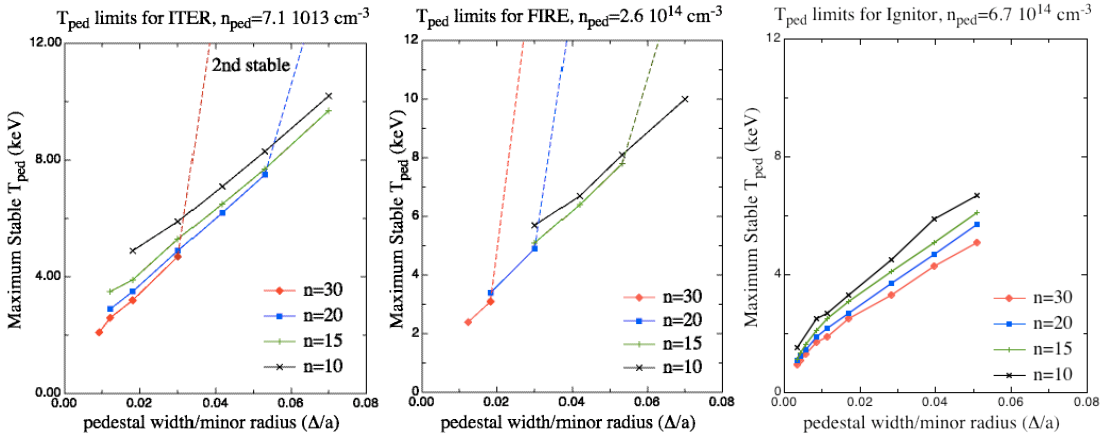

Figure 2: Maximum stable pedestal temperature for model equilibria of each device, as a function of the pedestal width. Stability boundaries for toroidal mode numbers n=10,15,20,30 are shown.

Because the candidate devices have different values of the pedestal density and magnetic field, it is useful to compare the pedestal stability constraints on normalized quantities. Figure 3 shows the pedestal stability constraints imposed by the most unstable of the studied wavelengths, in terms of the normalized pedestal β ($\beta_{Nped}=\beta_{ped}I/aB$), the pedestal β (β_{ped}), and the MHD alpha parameter at the pedestal center. The maximum stable β_{Nped} is similar at narrow pedestals for the three cases, but is higher for FIRE and ITER for wide pedestals, where high n modes are second stable in the more strongly shaped FIRE and ITER equilibria. Ignitor has the largest value of I/aB (Ignitor 1.86, ITER 1.42, FIRE 1.29) and therefore has slightly higher β_{ped} at a given Δ/a. The apparent trend is that the pedestal beta limits, as a function of Δ/a are remarkably similar for the three devices. Note that the maximum stable β value is not a constant, but rather decreases strongly with increasing pedestal width. This is because finite-n modes are sensitive to non-local equilibrium changes across the pedestal and not just the steepest local gradient, and also because the magnetic shear changes with pedestal width. Note also that the β value plotted in Figure 3c is the generalized β, which differs from the cylindrical value.

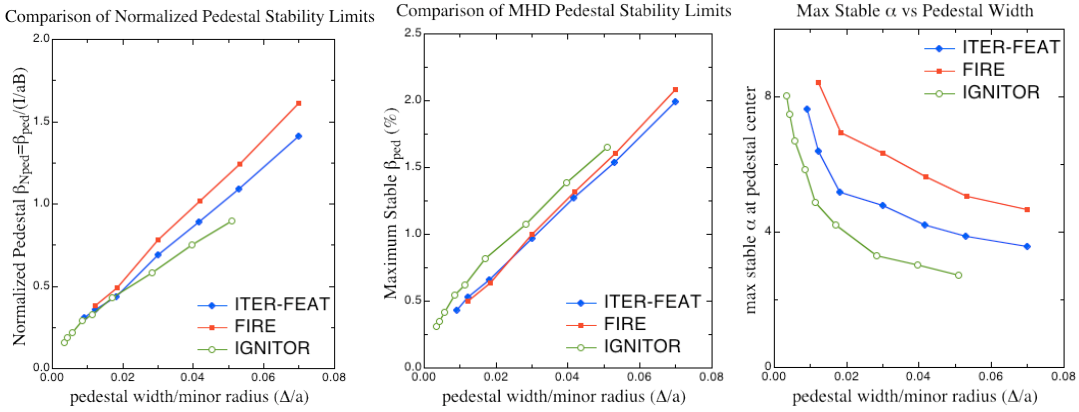

Figure 3: Comparison of pedestal stability limits for model equilibria of the three candidated devices, given in terms of (a) normalized pedestal beta, (b) pedestal beta, and (c) the MHD alpha parameter at the pedestal center; plotted against normalized pedestal width. The stability limit imposed by the most unstable of the studied n's (n=8,10,15,20,30) is shown.

II.c. Variation with triangularity and density

The pedestal stability results above employ equilibria with the standard set of equilibrium parameters given in Table 1. It is also of interest to study how these boundaries change with changes in the equilibria, particularly changes in parameters such as triangularity and density that are expected to be at least partially controllable in experiments.

The triangularity of the plasma cross-section has been found both theoretically and experimentally to significantly impact the pedestal [see e.g. Refs. 1-3,9,11]. In particular, higher triangularity generally improves the effective average curvature and increases pedestal beta limits at a given pedestal width. At high triangularity the peeling and ballooning branches of the instability begin to become decoupled, and second stability access can become possible for high n modes [14,13].

Figure 4a shows the results of a study in which the triangularity of the last closed flux surface (δ_a) is varied, while all other parameters in Table 1, and the pedestal width (5% of the poloidal flux, or $\Delta/a\sim0.03$) are held fixed. The pedestal stability limits increase strongly with triangularity, and begin to roll off around $\delta\sim0.5$. However, it should be noted that in these cases, the higher moments of the plasma shape, eg the squareness, are set to zero. It has been found in previous studies that stability limits continue to increase at very high values of δ if an optimized squareness is used [19].

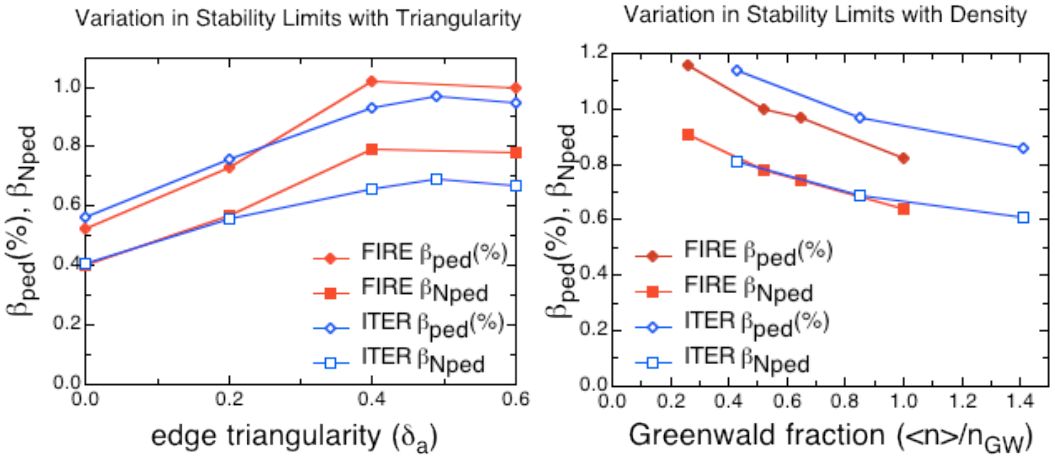

Figure 4: Variation in pedestal stability limits with triangularity and density for FIRE and ITER model equilibria. A fixed pedestal width of 5% of the poloidal flux ($\Delta/a\sim0.03$) is used and all parameters are from Table 1 except the indicated one which is varied.

Density also can impact pedestal stability limits. Because the current and resulting magnetic shear play an important role in determining pedestal stability limits, these limits have separate dependencies on density and temperature, not just the pressure [13]. Trading off density and

temperature at a given pressure alters the collisionality and the local value of the bootstrap current. A study of the variation of pedestal stability limits with density is shown in Figure 4b. Here the average density is varied with the pedestal density fixed at 0.71 of the average value, and the separatrix density fixed at 0.3 of the average. Lower density results in increased bootstrap current, lower shear, increased second stability access, and higher stability limits.

II.d. Unstable Mode Structure

The linear mode structure of the most unstable mode is expected to be related to the size of the resulting ELM, though nonlinear dynamics and scrape-off-layer physics likely play a significant role [see e.g., 7,10-14].

The mode structures of the limiting instabilities in the model equilibria for all three devices have a characteristic peeling-ballooning mode structure, localized to the outboard midplane, and extending radially somewhat beyond the pedestal. Lower n modes tend to have broader radial extent than higher n's, though the difference can be relatively small for a given equilibrium. Note however that, for the ITER and FIRE cases, lower n's are most unstable when the pedestal is wide, so there exists a clear correlation between the wavenumber of the most unstable mode and its radial extent (which is wider for wider pedestals). Example mode structures are given in Figure 5.

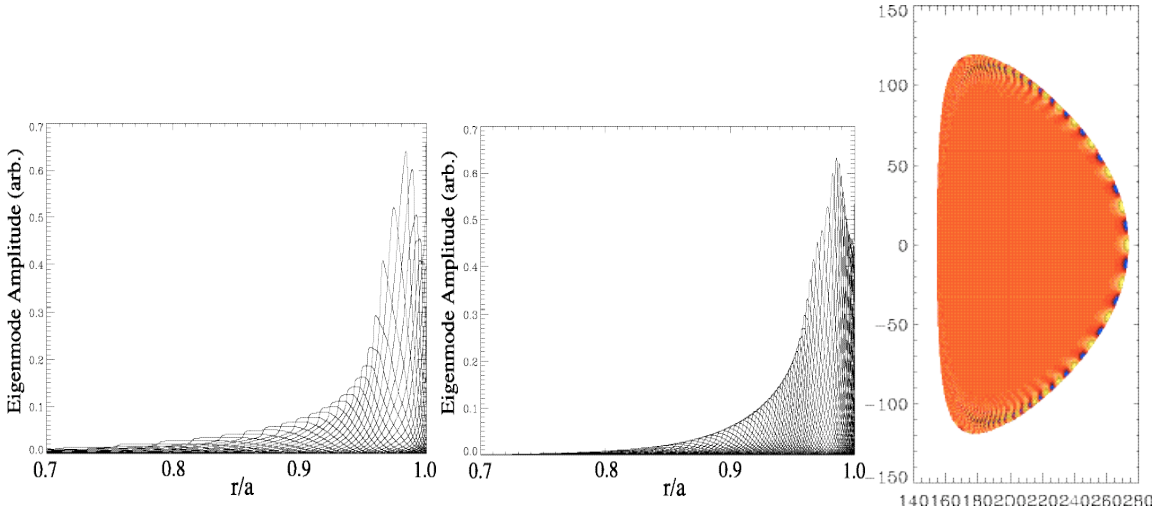

Figure 5: Comparison of radial eigenmode structures for (a) *n*=8 (b) n=20 in ITER model equilibrium with □/a=0.03, T_{ped}=6.2 keV. (c) 2D structure of an n=20 peeling-ballooning mode in FIRE model equilibrium with □/a=0.03, T_{ped}=5 keV.

III. Non-Ideal MHD Effects

A host of non-ideal and rotational physics can potentially modify the results of the previous section, including toroidal flow shear, finite resistivity, finite Larmor radius effects, kinetic resonance effects, and ExB shear.

Diamagnetic stabilization of short to intermediate wavelength instabilities has been identified as a potentially important piece of non-ideal physics in the pedestal regime [see e.g. Refs. 20-24]. A full treatment of diamagnetic effects requires a detailed kinetic or two-fluid formalism beyond the scope of this study. However, simple models can be used to estimate the impact of diamagnetic stabilization on the results from the previous section. The classic approach is to compare the calculated ideal MHD growth rate to the ion diamagnetic frequency, employing $\omega_{MHD}>\omega_{*pi}/2$ as the modified threshold for instability in the presence of diamagnetic stabilization [20,21]. This approach requires selecting a characteristic local value of ω_{*pi}, a quantity which varies rapidly over the pedestal. Here, we use the maximum value of $\omega_{*pi} \equiv \frac{cn}{en_i}\frac{\partial p_i}{\partial \psi}$ in the pedestal region divided by $\sqrt{2}$. Results obtained using this simple local model of diamagnetic stabilization are shown in Figure 6. [Note that compressionless values of ω_{MHD} are used here. These results are approximate and are intended only to provide an indication of the impact of diamagnetic effects.] One limitation of this local model is that it assumes a constant level of diamagnetic stabilization over the full radial extent of the mode, which can extend beyond the pedestal. For narrow pedestals this can lead to a significant overestimate of the stabilizing effect. A modification suggested by B. Rogers and J. Drake [25] allows a smooth transition from the regime where the pedestal is much wider than the mode to the regime in which it is much narrower than the mode. The $\omega_{*pi}/2$ term given above is multiplied by a factor of $1/(1+1/k_\psi L_p)$. Here k_ψ is determined on the outer midplane, and L_p is taken to be approximately the pedestal half width. Results with this modified diamagnetic stabilization model are also given in Figure 6. [Stability limits at narrow widths in the presence of the diamagnetic stabilization are more challenging to calculate, and are not presented in the figure, but this should not be taken as an indication that no stability limit exists for these cases.]

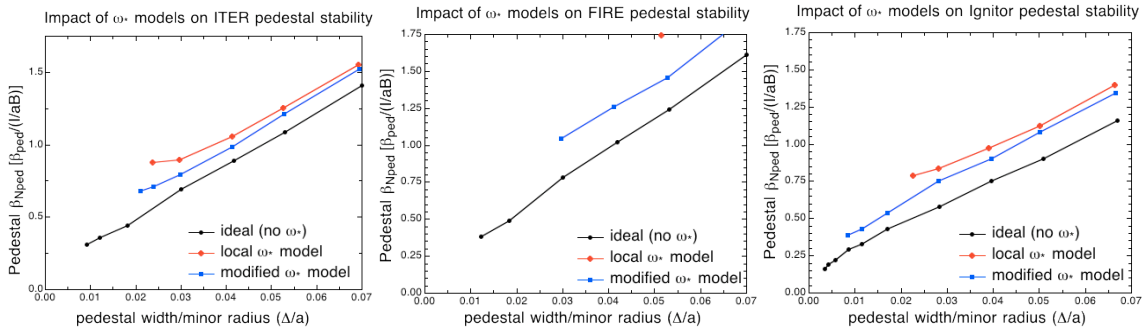

Figure 6: Stability constraints (from n=8,10,15,20,30 modes) on the normalized pedestal beta as a function of pedestal width, including results with the local $\omega_{MHD}>\omega_{*pi}/2$ model of diamagnetic stabilization, and with the modified model.

IV. Summary of Pedestal Stability Study

A set of model equilibria with varying pedestal width (Δ) and height have been constructed for each device, and constraints imposed by intermediate n=8-30 MHD modes have been assessed using the ELITE code. The calculated stability bounds on β_{ped} vs Δ/a are similar between the machines. The maximum stable pedestal height (β_{ped}) is a strong function of the width, though notably sub-linear particularly at narrow widths. The maximum stable height is a strong function

of triangularity, and a weaker function of density. Intermediate to high n modes are found to be the limiting instability, and calculated mode structures, which are expected to be related to the ELM depth, extend inward somewhat beyond the pedestal. Diamagnetic effects on the stability bounds are assessed with a local model ($\beta > \beta_{*pi}/2$), and with a modified local model which takes into account the finite ratio of mode width to pedestal width. Diamagnetic effects, as modeled by these simple models, are found to significantly increase the ideal MHD bounds and to shift the limiting mode to longer wavelengths.

V. Implications

V.a. Connection to Core Transport Models and Empirical Pedestal Scaling

Core transport modeling is discussed in the transport section of this report, and only the connection between core transport and pedestal conditions will be briefly considered here.

Previous study using the GLF23 transport model has found that pedestal β values in the vicinity of 0.5-1% are required for good performance. More specifically, GLF23 simulations predict a value of β_{Nped}~0.43 is required for Q=10 at P_{aux}=20 MW on ITER, and a value of β_{Nped}~0.60 is required for Q=10 at P_{aux}=10 MW on FIRE [26]. As shown in Figure 3a, these pedestal heights are found to be ideal MHD stable to the studied range of modes (n=8-30) for pedestal widths of $\Delta/a > \sim 0.025$. Pedestal widths of this size fall within the observed range on several machines, however, they tend to be toward the upper end of the range.

It should also be noted that optimization of the plasma cross-section shape and density can significantly increase the pedestal stability constraints given in Figure 3. Furthermore, the simple models suggest that diamagnetic stabilization will significantly increase the pedestal stability limits, as shown in Figure 6, allowing the required pedestal heights at significantly narrower widths.

However, it is not clear that the pedestal width should scale linearly with *a*. A number of studies of empirical pedestal width scaling have been carried out [see e.g. 1-3,27], with varying results, but often a width scaling with a low power of the ion poloidal gyroradius or the poloidal beta, or with the neutral particle penetration depth (for the density width), is found. A number of factors complicate the process of arriving at a useful empirical pedestal scaling. First, few machines directly measure the pedestal width accurately, and therefore width scalings are often attempted by dividing the observed pedestal height by some measure of the "ideal MHD critical gradient." It should be clear from the preceding sections that there is in general no ideal MHD critical gradient which is independent of the pedestal width. Also, the scaling of ideal MHD limits can be complex, due to the role of the bootstrap current and the separate dependencies on density and temperature that it introduces, and due to finite-n modes having finite radial width and sensitivity to non-local features of the equilibrium. Hence, width scalings derived by dividing observed pedestal heights by fixed "ideal MHD critical gradients" are at best very rough approximations. Additionally, the observed scalings in which the pedestal width is observed to increase with factors such as gyroradius or β_p, which increase with pedestal height, must be studied carefully. If indeed the pedestal is constrained by MHD stability, the pedestal height is expected to increase with pedestal width (and vice versa), and therefore scalings that describe the width increasing

with height may need to be quite precise in order to provide information on the actual physics limiting the width.

On existing machines, a wide range of pedestal conditions are generally achievable. Values of $\beta_{Nped} > \sim 0.7$ have been achieved on multiple machines [1-3,28]. It therefore seems reasonable to expect that the burning plasma candidates will be able to achieve the required range of pedestal heights, though this may require significant work on pedestal optimization experiments.

V.b. ELM Size

Achieving high pedestals in the burning plasma candidate devices is significantly complicated by the simultaneous requirement of small ELMs. In present machines, it is often observed that large ELMs are found at the highest pedestal regimes [3,7,28-30].

In the stability study, both ITER and FIRE are found to be near the threshold for significant second stability access in the pedestal. This suggests that, via small modifications to the shape or other variables, that the machines could move in and out of the second stable pedestal regime, and explore the resulting expected tradeoffs between high pedestal and larger ELMs.

The most unstable mode structures found in the stability study extend somewhat beyond the pedestal region, similar to results of analysis on present machines. The mode structures are wider at large pedestal widths and slightly wider when longer wavelengths are most unstable. This suggests somewhat larger ELMs for wide pedestal, strongly second stable cases, but the details are highly uncertain.

It has been observed that ELM size is reduced at higher densities [29,30]. Whether this physics is tied to the increase in pedestal collisionality, increased Greenwald density fraction, or increased parallel transport time in the scrape-off-layer, remains an active area of study. The burning plasma candidates likely will need to operate at low collisionality at the top of the pedestal, but will have high collisionality/long parallel transport time in the SOL, and may operate at high Greenwald density fraction.

The stability study above, as well as observations on existing devices, suggests that shaping flexibility, and the ability to vary the density, are desirable in order to allow optimization of the pedestal and ELMs. In particular, the benefits of operating in first versus second stable pedestal regimes could be explored by varying the shape in a flexible, strongly shaped device. Also, the benefits of operating at low Greenwald fraction (predicted higher pedestals) could be contrasted with possible benefits (smaller ELMs, divertor) of high density operation. An ability to vary the current in the pedestal region, for example via off-axis current drive, may also aid in controlling ELM and pedestal behavior.

In conclusion, pedestal physics, particularly the physics setting the pedestal width, is not fully understood and progress is needed to allow detailed quantitative predictions of pedestal height and ELM characteristics. However, studies have been undertaken using available tools to evaluate MHD stability constraints on the pedestals of model equilibria as a feasibility check on the pedestal heights required by core transport models for good performance, and to provide

input for models of ELMs. The results of the stability study, particularly if models of diamagnetic stabilization are considered, do not suggest that the required pedestal heights are infeasible. They suggest that ELM behavior may be similar to that observed on present devices, and that effort may be needed to develop high pedestal, small (or no) ELM regimes during the early operation phases of the proposed devices.

References

[1] Hubbard, A.E., Plasma Phys. Control. Fusion 42 (2000) A15
[2] Hatae T., Sugihara, M., Hubbard, A.E., Nucl. Fusion 41 (2001) 285
[3] Osborne, T.H., Ferron, J.R., Groebner, R.J., et. al, Plasma Phys. Control. Fusion 42 (2000) A175
[4] Zohm, H., Plasma Phys. Contol. Fusion 38 (1996) 105
[5] Connor, J.W., Plasma Phys. Control. Fusion 40 (1998) 191
[6] Suttrop, W., Plasma Phys. Contol. Fusion 42 (2000) A1
[7] Lao, L.L., Plasma Phys. Control. Fusion 42 (2000) A51
[8] Snyder, P.B. and Wilson, H.R., Contrib. Plasma Physics 42 (2002) 258.
[9] Huysmans, G.T.A., Hender, T.C., Alper, P., et. al, Nucl. Fusion 39 (1999) 1489; M. Becoulet et al., Plasma Phys. Control. Fusion 44 (2002) A103.
[10] Mossessian, D., Snyder, P.B., Greenwald, M., et al, Plasma Phys. Control. Fusion 44 (2002) 423-437
[11] Ferron, J.R., Chu, M.S., Jackson, G.L., et al., Phys. Plasmas 7 (2000) 1976; Strait, E.J., et al., Proc. 20th EPS Conf. on Plasma Physics and Controlled Fusion Research (Lisbon, Portugal) vol 17C part 1 p 211 (1993); Ferron, J.R., et al., Proc. 22nd EPS Conf. on Plasma Physics and Controlled Fusion Research (1995); Osborne, T.H., et al., EPS Conf. Plas. Phys. Contr. Fusion (1997)
[12] Saarelma, S., Gunter, S., Kurki-Suonio, T., Zehrfeld, H.-P., Plasma Phys. Control. Fusion 42 (2000) A139
[13] Snyder, P.B., Wilson, J.R. Ferron et al., Phys. Plasmas **9** (2002) 2037.
[14] Connor, J.W., Hastie, R.J., Wilson, H.R., and Miller, R.L., Phys. Plasmas 5 (1998) 2687; Hegna, C.C., Connor, J.W., Hastie, R.J., and Wilson, H.R., Phys. Plasmas 3 (1996) 584; Wilson, H.R., and Miller, R.L., Phys. Plasmas 6 (1999) 873.
[15] Sauter, O., Angioni, C., and Lin-Liu, Y.R., Phys. Plasmas 6 (1999) 2834.
[16] Wilson, H.R., Snyder, P.B., Huysmans, G.T.A., and Miller, R.L., Phys. Plasmas **9** (2002) 1277.
[17] Bernard, L.C., et. al, Comp. Phys. Commun. 24 (1981) 377
[18] Mikailovskii, A.B., Huysmans, G.T.A., Sharapov, S.E., Kerner, W., Plasma Phys. Rep. 23 (1997) 844
[19] Turnbull, A.D., Lin-Liu, Y.R, Miller, R.L., et al., Phys Plasmas 6 (1999) 1113; DIII-D Five Year Plan Report (2002).
[20] Roberts, K.V., Taylor, J.B., Phys. Rev. Lett. 8 (1962) 197
[21] Tang, W.M., Dewar, R.L., Manickam, J., Nucl. Fusion 22 (1982) 1079
[22] Hahm, T.S., Diamond, P.H., Phys. Fluids 30 (1987) 133
[23] Rogers, B.N., Drake, J.F. Phys. Plasmas 6 (1999) 2797
[24] Hastie, R.J., Catto, P.J., Ramos, J.J., Phys. Plasmas 7 (2000) 4561
[25] Rogers, B.N. and Drake, J.F., private communication (2002). A similar model is employed in the context of a circular s-alpha model in Ref. [23].
[26] Kinsey, J. et al., Sherwood conference (2002); R. Waltz et al. Snowmass P4 group report (2002).
[27] Groebner, R.J., Mahdavi, M.A., Leonard, A.W., et al., Plasma Phys. Control. Fusion 44 No 5A (2002) A265.
[28] ITPA pedestal database
[29] Leonard, A.W., Groebner, R.J., Mahdavi, M.A. et al., Plasma Phys. Control. Fusion 44 No 6 (2002) 945.
[30] Loarte, A., et al. "ELM Energy and Particle Losses and their Implications for Next Step Devices and Fusion Reactors", IAEA TCM on Divertor Concepts, September 11-14, 2001, Aix-en-Provence, France.